Journal of the Egyptian Mathematical Society 25 (2017) 238–251

Contents lists available at ScienceDirect

Journal of the Egyptian Mathematical Society

journal homepage: www.elsevier.com/locate/joems

Original Article

Cilia walls influence on peristaltically induced motion of magneto-fluid through a porous medium at moderate Reynolds number: Numerical study

R.E. Abo-Elkhair, Kh.S. Mekheimer*, A.M.A. Moawad

Mathematical Department, Faculty of Science Al-Azhar University, Nasr City 11884, Cairo, Egypt

ARTICLE INFO

Article history:
Received 13 July 2016
Revised 11 November 2016
Accepted 3 January 2017
Available online 23 January 2017

2014 MSC:
76D05
76S05
76W05
76Z05

Keywords:
Oscillatory flow
Metachronal beating of cilia
Magnetic field
Porous medium
ADM

ABSTRACT

This article addresses, effects of a magneto-fluid through a Darcy flow model with oscillatory wavy walled whose inner surface is ciliated. The equations that governing the flow are modeled without using any approximations. Adomian Decomposition Method (ADM) is used to evaluate the solution of our system of nonlinear partial differential equations. Stream function, velocity and pressure gradient components are obtained by using the vorticity formula. The effects for our arbitrary physical parameters on flow characteristics are analyzed by plotting diagrams and discussed in details. With the help of stream lines the trapping mechanism has also been discussed. The major outcomes for the ciliated channel walls are: The axial velocity is higher without a ciliated walls than that for a ciliated walls and an opposite behaviour is shown near the ciliated channel walls. The pressure gradients in both directions are higher for a ciliated channel walls. More numbers of the trapped bolus in the absent of the eccentricity of the cilia elliptic path.

1. Introduction

Oscillatory wavy walled (Peristalsis) play an important phenomena in the transport of biofluids and involved in many bio-mechanical systems. Also, pumping phenomena with peristalsis is used for pumping corrosive materials so as to prevent direct contact of the fluid with the pump's internal surfaces. Moreover, by using the principle of peristalsis, some bio-mechanical instruments, as heart-lung machine have been simulated. Numbers of analytical [1–12], numerical and experimental [13–17] studies of peristaltic flows for different fluids have been discussed.

The effect of magnetic field and Darcy medium on the peristaltic mechanisms are important in connection with specific problems of the movements of the conductive physiological fluids, see [18–25].

Cilia, hair resembles animated appendages, presented in the respiratory, digestive and reproductive system of males and females and the nervous system in all categories of the animal kingdom. Cilia motion plays an important role in physiological processes such as locomotion, feeding, circulation, breathing, and reproduction. The cilia beatings, being well coordinated, generate a metachronal wave. The envelope of cilia tips, forming the metachronal wave, acts as an extensible wall with a tendency of forward motion always in the same direction. Some various studies about a cilia transport have been achieved by references [26–36].

No attempt has been made yet to study and solve this model by using the ADM method without any wavy walls approximations. Therefore in this paper, we will present the influence of the magnetic field and Darcy medium on peristaltic flow due to the cilia motion. The governing non-linear partial differential equations of this model have been solved with the ADM method. This method has already been used for the solutions of several other problems [43–46]. The impact of all the physical parameters is discussed and plotted. The paper is organized as follows. Section 2 includes the explanation of ADM briefly. The physical modeling statement with geometry of our problem is presented in Section 3. The Adomian Decomposition Method for solving our system equations is given in Section 4. In Section 5, we discussed in details the results we have obtained and the effects for our arbitrary physical parameters on the flow characteristics. Major findings of our model are included in the last section.

* Corresponding author.
E-mail addresses: elkhair33@azhar.edu.eg (R.E. Abo-Elkhair), kh_mekheimer@azhar.edu.eg, kh_mekheimer@yahoo.com (Kh.S. Mekheimer), ali_moawad2008@azhar.edu.eg (A.M.A. Moawad).

http://dx.doi.org/10.1016/j.joems.2017.01.001

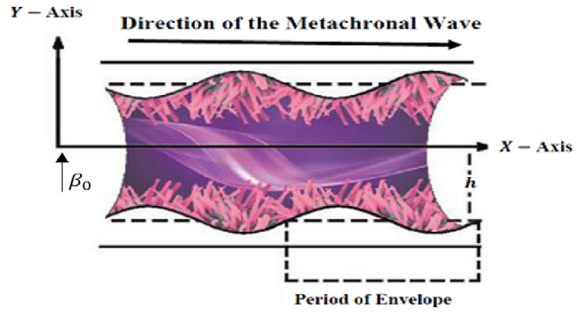

Fig. 1. Geometry of the problem.

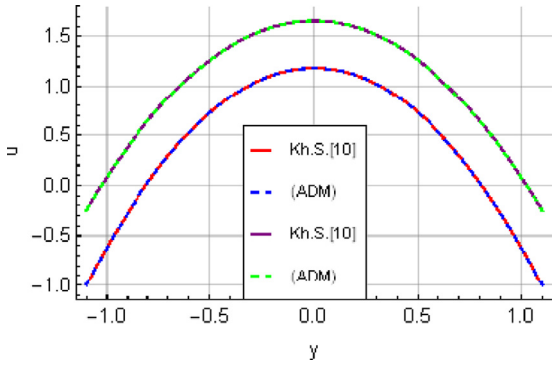

Fig. 2. Comparison between present method($\alpha \neq 0$, $R_e \neq 0$) and result obtained by Mekheimer [10]. (a) $\phi = 0.1$, Q = 0.5; (b) $\phi = 0.3$, Q = 1 .

2. The adomian decomposition method(ADM)

To explain this method [37–42] , we consider the following differential equation

$$Lu + Ru + Nu = g(x), \tag{1}$$

with prescribed conditions. In the above equation $u(x)$ is unknown scalar function, L is the highest-order derivative which is assumed to be easily invertible, R is a linear differential operator of order less than L, Nu represents the nonlinear terms, and g is an inhomogeneous term. Applying the inverse operator L^{-1} to both sides of Eq. (1), and using the given conditions we have

$$u(x) = f(x) - L^{-1}(Ru) - L^{-1}(Nu), \tag{2}$$

in which the function $f(x)$ represents the terms arising from the integration of $g(x)$ and then using prescribed intial or boundary conditions. For examble, if $L = \frac{d^3}{dx^3}$, then L^{-1} is a three-fold integration, and

$$f(x) = u(0) + xu'(0) + \frac{x^2}{2!}u'''(0) + L^{-1}g$$

.

The linear term $u(x)$ in terms of an infinite sum of components u_m is decomposed through the following equation

$$u(x) = \sum_{m=0}^{\infty} u_m(x). \tag{3}$$

The nonlinear operator Nu can be decomposed into a infinite series of polynomials as

$$Nu = \sum_{m=0}^{\infty} A_m(x). \tag{4}$$

The components of $u(x)$ can be determined recursively. $A_m(x)$ are the Adomian polynomials of u_0, u_1, $u_2 \cdots$, u_m and satify

$$A_m = \frac{1}{m!}\frac{d^m}{d\lambda^m}\left[N\left(\sum_{i=0}^{\infty}\lambda^i u_i\right)\right]_{\lambda=0}, \qquad m = 0, 1, 2\cdots \tag{5}$$

From Eqs. (2)-(4) we have

$$\sum_{m=0}^{\infty} u_m(x) = f(x) - L^{-1}\left(R\sum_{m=0}^{\infty} u_m\right) - L^{-1}\left(R\sum_{m=0}^{\infty} A_m\right). \tag{6}$$

The above equation easily gives

$$\begin{aligned} u_0 &= f(x), \\ u_{m+1} &= L^{-1}(Ru_m) - L^{-1}(A_m), \qquad m \geq 0. \end{aligned} \tag{7}$$

All components are determinable since A_0 depends only on u_0, A_1 depends on u_0, u_1, etc. Moreover, since the series is commonly rapidly convergent, the m-term partial sum $\phi_m = \sum_{i=0}^{m-1} u_i$ could be the practical solution.

Table 1
Comparison of longitude velocity distribution for present work when $\alpha = 0.01$, $R_e = 0.01$ and work obtained by Mekheimer [10] for fixed values of $\phi = 0.1$, $q = 0.5$.

y	u(x,y) Present work	u(x,y) Mekheimer [10] with long wavelength approximation	|error|
−1.1	−1	−1	0
−0.9	−0.278794	−0.278738	−0.0000566376
−0.7	0.298227	0.298272	−0.0000445125
−0.5	0.731027	0.731029	$-1.91459*10^{-6}$
−0.3	1.01958	1.01953	0.0000424383
−0.1	1.16386	1.16379	0.0000694011
0	1.18189	1.18182	0.0000729958

Regarding the convergence of the decomposition method and the detailed description of the Adomian decomposition and the modified decomposition algorithms, we refer the readers to the studies [43–46].

3. Statement of physical model

Let's take in our consideration an incompressible MHD flow with a Darcy flow model in symmetric channel. Flow occurs due to the metachronal wave which is produced due to collective beating of the cilia with constant speed c along the walls of the channel whose inner surface is ciliated (Fig. 1). The plates of the channel are assumed to be electrically insulated. We assume that a uniform magnetic field strength β_0 is applied in the transverse direction to the direction of the flow and the induced magnetic field is assumed to be negligible. The geometry of the envelope of cilia tips and the flow of fluid are represented in two coordinate systems; one, fixed in the space, is (X, Y) and another is (x', y') moving to the right with a speed c relative to the fixed one. The two coordinate systems are connected with the relation.

$$X = x' + ct, \qquad Y = y', \qquad U = u' + c, \qquad V = v', \tag{8}$$

where (U, V) and (u', v') are components of velocity in the fixed and moving systems respectively.

The channel walls surface (in fixed systems) are given by (Fig. 1):

$$H(X, t) = \pm\left[h + \epsilon\cos\left[\frac{2\pi}{\lambda}(X - ct)\right]\right], \tag{9}$$

or (in moving systems) written as:

$$\eta'(x') = \pm\left[h + \epsilon\cos\left[\frac{2\pi}{\lambda}x'\right]\right], \tag{10}$$

where, t is time, λ is wavelength, ϵ is the wave amplitude, h is mean distance of the wall from the central axis and c is wave velocity of the metachronal wave. Following Sleigh [26], the cilia tips

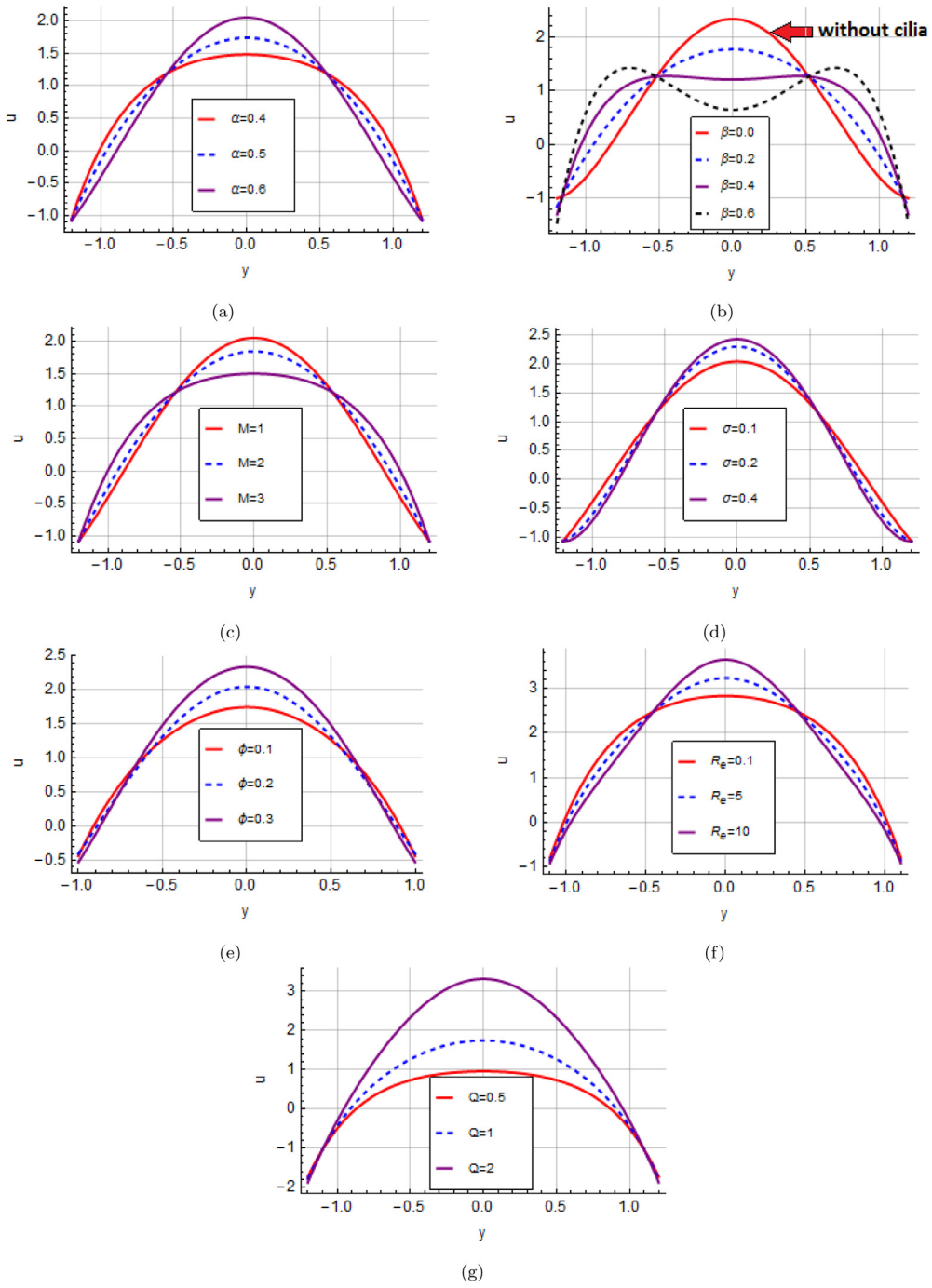

Fig. 3. Longitude velocity distribution for different values of physical parameters.

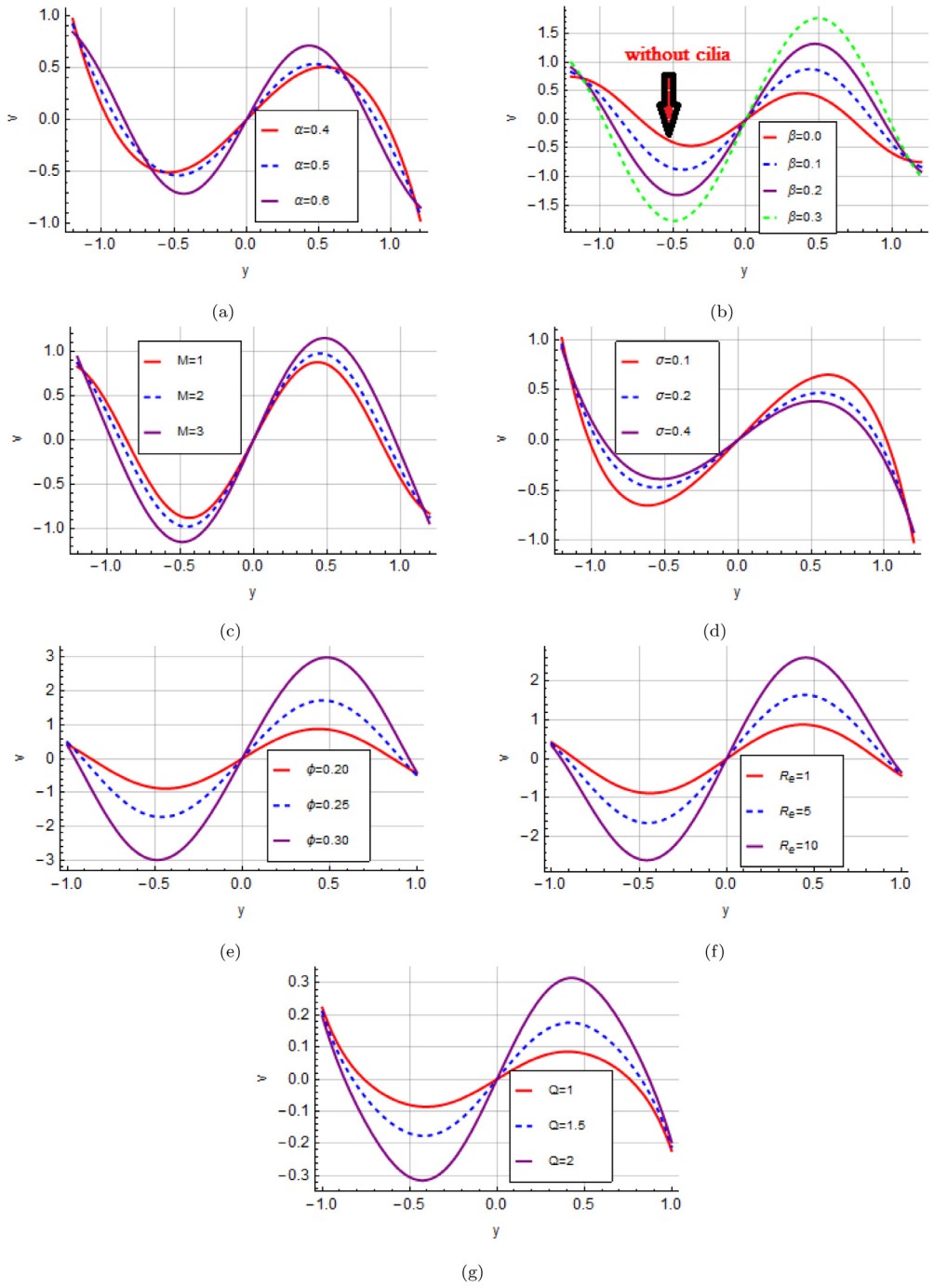

Fig. 4. Vertical velocity distribution for different values of physical parameters.

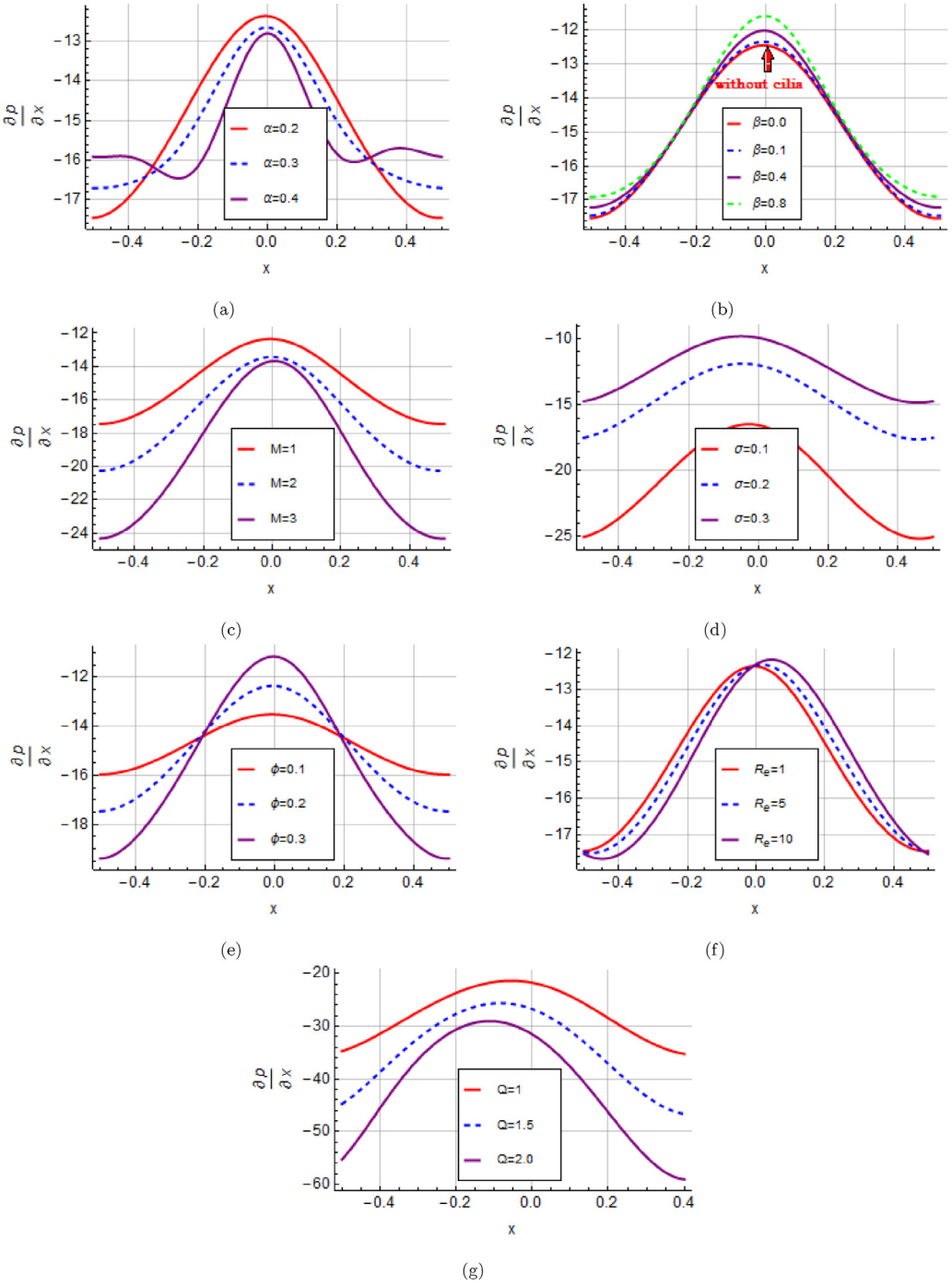

Fig. 5. Variation of pressure gradient ($\frac{\partial p}{\partial x}$) for different values of physical parameters.

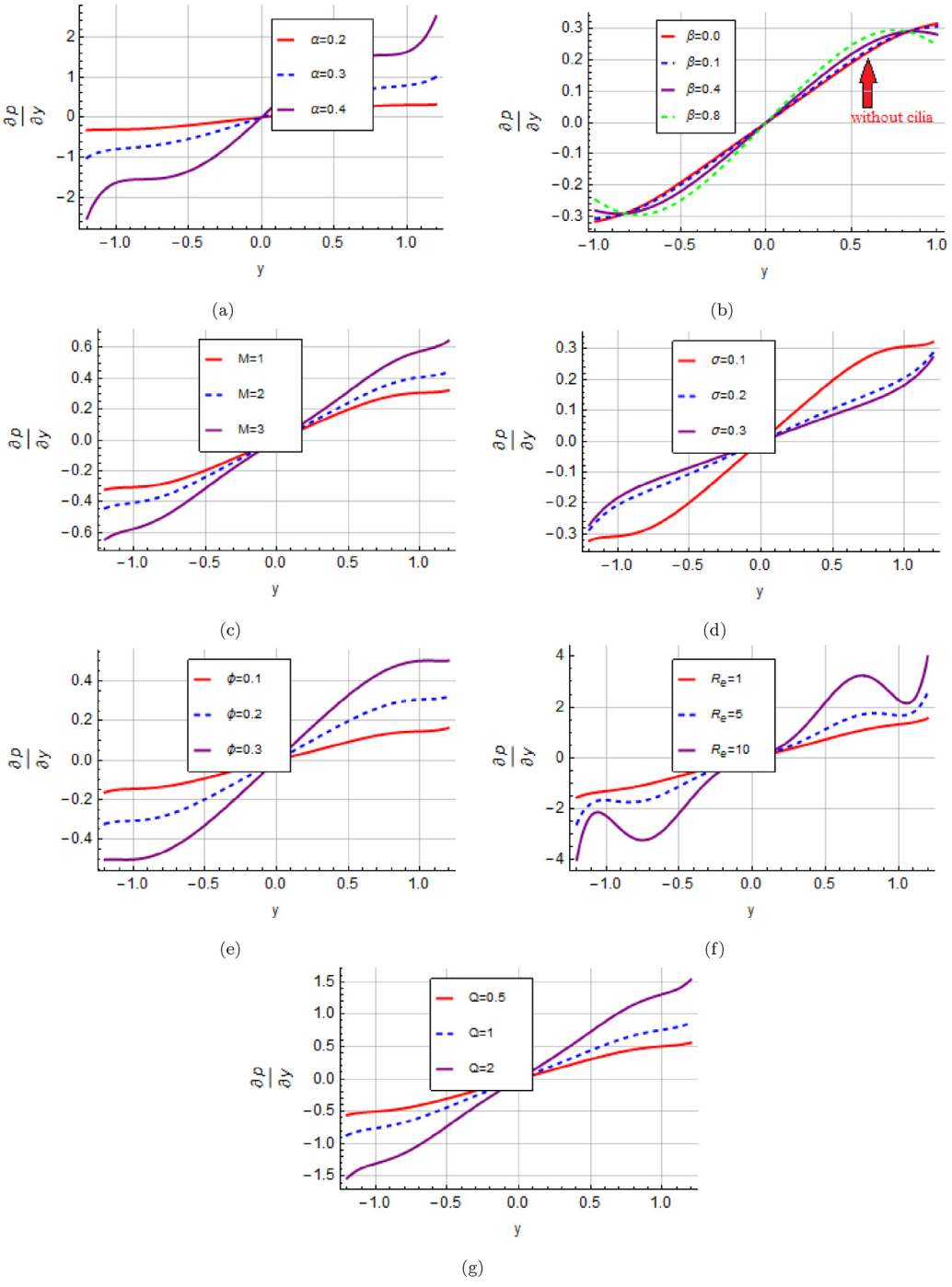

Fig. 6. Variation of pressure gradient ($\frac{\partial p}{\partial y}$) for different values of physical parameters.

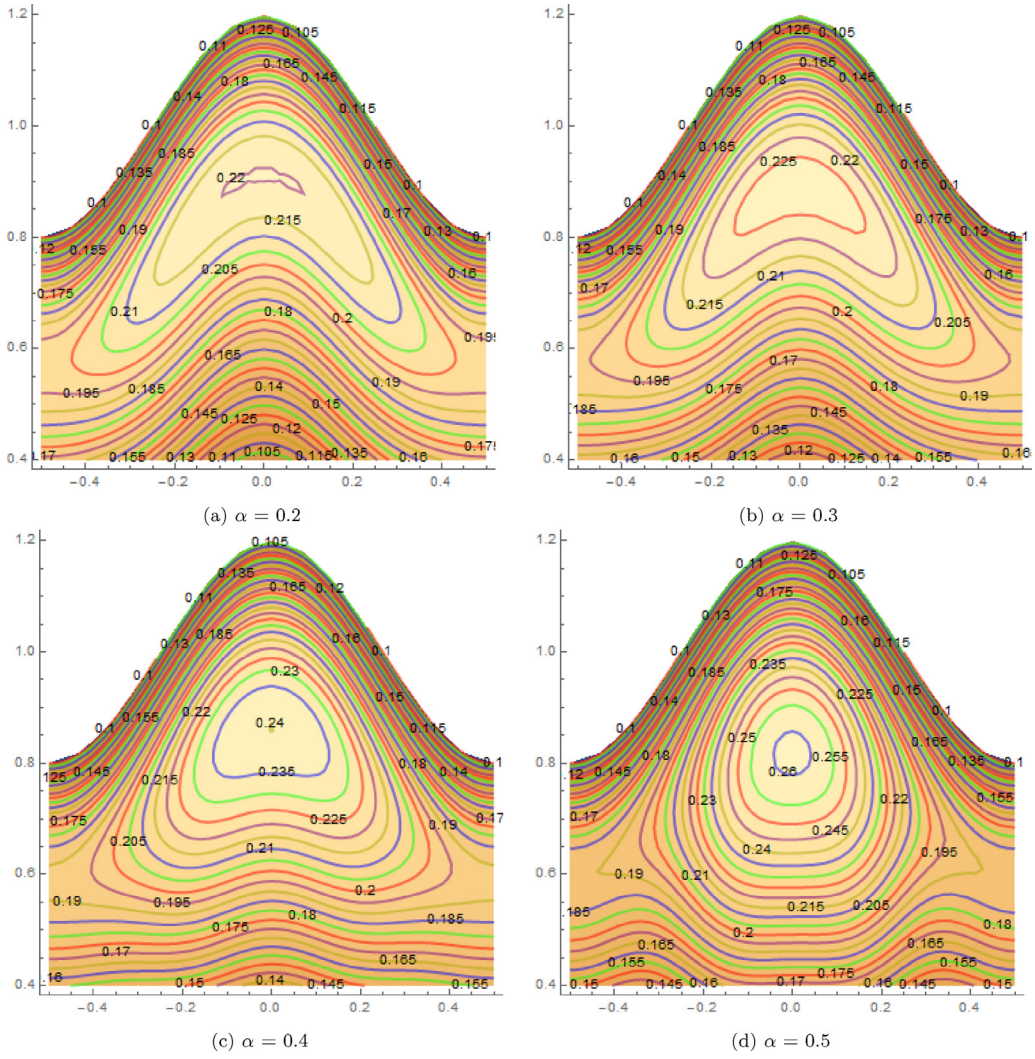

(a) $\alpha = 0.2$ (b) $\alpha = 0.3$

(c) $\alpha = 0.4$ (d) $\alpha = 0.5$

Fig. 7. Streamlines for different values of α and other parameters are ($\phi = 0.2$, $R_e = 0.1$, $M = 1$, $\sigma = 0.1$, $\beta = 0.1$, $Q = 0.1$).

are assumed to move in elliptic paths so that the horizontal position of a cilia tip is given as :

$$F(X,t) = X_0 + \beta\epsilon \sin\left[\frac{2\pi}{\lambda}(X - ct)\right], \tag{11}$$

where, X_0 is a reference position of the cilia and β is a measure of the eccentricity of the elliptic path.

Using the following nondimensional variables:

$$x = \frac{x'}{\lambda}, \quad y = \frac{y'}{h}, \quad u = \frac{u'}{c}, \quad v = \frac{\lambda}{ch}v', \quad \psi = \frac{\psi'}{ch},$$
$$\omega = \frac{h}{c}\omega', \quad Q = \frac{Q'}{ch}, \quad p = \frac{h^2}{\mu c\lambda}p', \quad \eta = \frac{\eta'}{h}, \tag{12}$$

where, the amplitude ratio "ϕ", the wave number "α", Hartmann number "M", the porosity parameter "σ" and the Reynolds number "R_e", are defined by

$$\phi = \frac{\epsilon}{h}, \quad \alpha = \frac{h}{\lambda}, \quad M = \sqrt{\frac{\sigma_0}{\mu}}\beta_0\, h, \quad R_e = \frac{\rho ch}{\mu}, \quad \sigma = \frac{K}{h^2}. \tag{13}$$

The equations of motion [1,22,25] for a moving system in the dimensionless form become:

$$\frac{\partial u}{\partial x} + \frac{\partial v}{\partial y} = 0, \tag{14}$$

$$R_e\alpha\left[u\frac{\partial u}{\partial x} + v\frac{\partial u}{\partial y}\right] = -\frac{\partial p}{\partial x} + \left[\alpha^2\frac{\partial^2 u}{\partial x^2} + \frac{\partial^2 u}{\partial y^2}\right] - M^2(u+1) - \frac{1}{\sigma}(u+1), \tag{15}$$

$$R_e\alpha^3\left[u\frac{\partial v}{\partial x} + v\frac{\partial v}{\partial y}\right] = -\frac{\partial p}{\partial y} + \alpha^2\left[\alpha^2\frac{\partial^2 v}{\partial x^2} + \frac{\partial^2 v}{\partial y^2}\right] - \frac{\alpha^2}{\sigma}v. \tag{16}$$

Also, the configuration of the peristaltic wall can be represented by:

$$\eta(x) = 1 + \phi\cos[2\pi x], \tag{17}$$

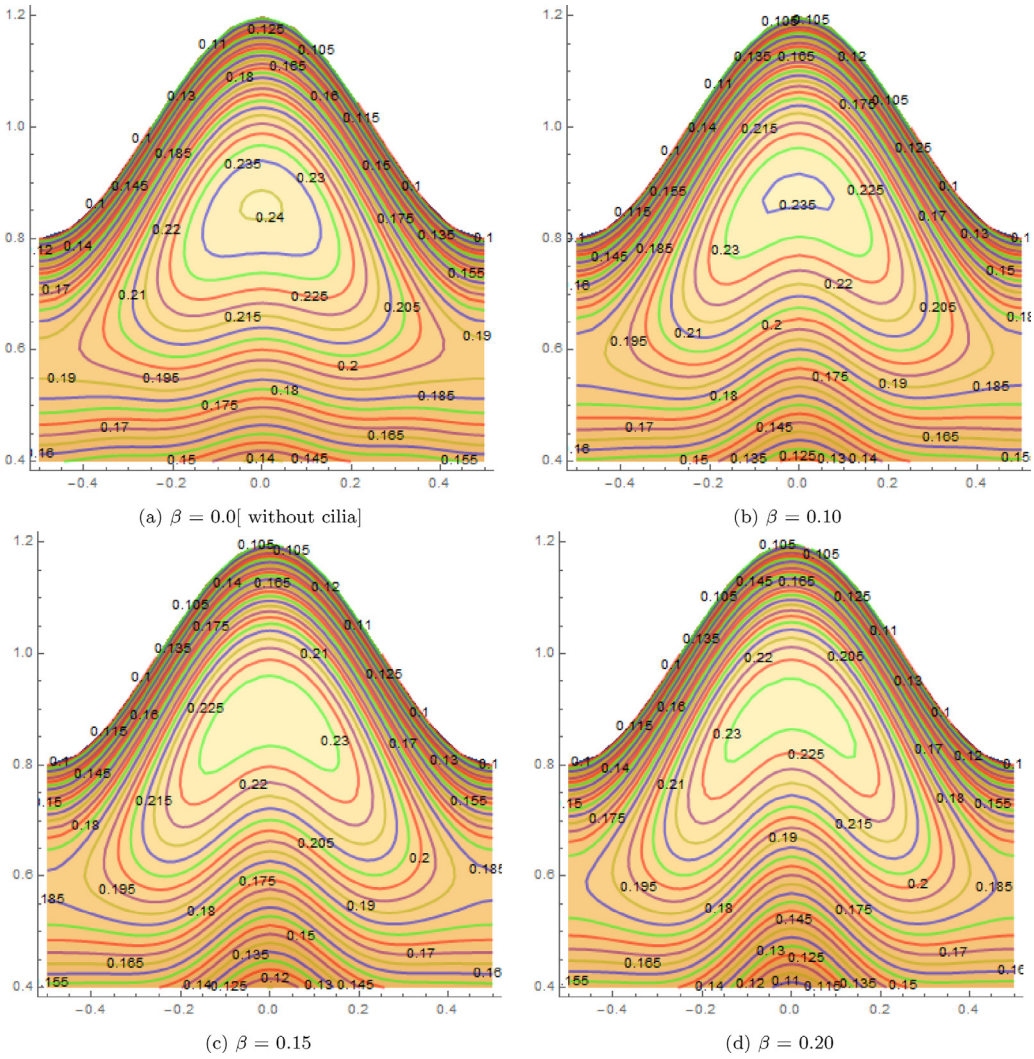

(a) $\beta = 0.0$[without cilia] (b) $\beta = 0.10$

(c) $\beta = 0.15$ (d) $\beta = 0.20$

Fig. 8. Streamlines for different values of β and other parameters are ($\alpha = 0.4$, $\phi = 0.2$, $R_e = 0.1$, $M = 1$, $\sigma = 0.1$, $Q = 0.1$).

The boundary conditions can be expressed as:

$$\begin{aligned} &v = 0, \quad \frac{\partial u}{\partial y} = 0, \quad \psi = 0 \quad \text{at } y = 0, \\ &u = -1 - 2\pi\phi\alpha\beta\cos[2\pi x], \quad v = 2\pi\alpha\phi\sin[2\pi x], \\ &\psi = Q \quad \text{at } y = \eta(x). \end{aligned} \tag{18}$$

The stream function ψ and vorticity ω are defined by:

$$u = \frac{\partial \psi}{\partial y}, \qquad v = -\frac{\partial \psi}{\partial x}, \qquad \omega = \alpha^2 \frac{\partial v}{\partial x} - \frac{\partial u}{\partial y}. \tag{19}$$

By eliminating the pressure, the governing equations and boundary conditions in terms of ψ will takes the form

$$\begin{aligned} \frac{\partial^4 \psi}{\partial y^4} = R_e\alpha &\left[\left(\frac{\partial \psi}{\partial y}\right)\left(\frac{\partial^3 \psi}{\partial x \partial y^2} + \alpha^2 \frac{\partial^3 \psi}{\partial x^3}\right)\right. \\ &\left. -\left(\frac{\partial \psi}{\partial x}\right)\left(\frac{\partial^3 \psi}{\partial y^3} + \alpha^2 \frac{\partial^3 \psi}{\partial x^2 \partial y}\right)\right] \\ &-\left[\alpha^4 \frac{\partial^4 \psi}{\partial x^4} + 2\alpha^2 \frac{\partial^4 \psi}{\partial x^2 \partial y^2}\right] + M^2 \frac{\partial^2 \psi}{\partial y^2} \\ &+\frac{1}{\sigma}\left(\frac{\partial^2 \psi}{\partial y^2} + \alpha^2 \frac{\partial^2 \psi}{\partial x^2}\right), \end{aligned} \tag{20}$$

and the no-slip condition or the symmetry condition on the planes $y = 0$ and $y = \eta(x)$ can be expressed as follows:

$$\begin{aligned} &\psi = 0, \quad \frac{\partial^2 \psi}{\partial y^2} = 0, \quad \frac{\partial \psi}{\partial x} = 0 \quad \text{at } y = 0, \\ &\psi = Q, \quad \frac{\partial \psi}{\partial y} = -1 - 2\pi\phi\alpha\beta\cos[2\pi x], \\ &\frac{\partial \psi}{\partial x} = 2\pi\phi\alpha\sin[2\pi x] \quad \text{at } y = \eta(x). \end{aligned} \tag{21}$$

4. ADM solution

For the solution of Eq. (20) with the boundary conditions (21), we use ADM , we write Eq. (20) in operator form

$$\begin{aligned} \psi = L_y^{-1}&\left(R_e\alpha\left[\left(\frac{\partial \psi}{\partial y}\right)\left(\frac{\partial^3 \psi}{\partial x \partial y^2} + \alpha^2 \frac{\partial^3 \psi}{\partial x^3}\right)\right.\right. \\ &\left.\left. -\left(\frac{\partial \psi}{\partial x}\right)\left(\frac{\partial^3 \psi}{\partial y^3} + \alpha^2 \frac{\partial^3 \psi}{\partial x^2 \partial y}\right)\right]\right) \\ &-L_y^{-1}\left(\left[\alpha^4 \frac{\partial^4 \psi}{\partial x^4} + 2\alpha^2 \frac{\partial^4 \psi}{\partial x^2 \partial y^2}\right] + M^2 \frac{\partial^2 \psi}{\partial y^2}\right. \\ &\left.+\frac{1}{\sigma}\left(\frac{\partial^2 \psi}{\partial y^2} + \alpha^2 \frac{\partial^2 \psi}{\partial x^2}\right)\right). \end{aligned} \tag{22}$$

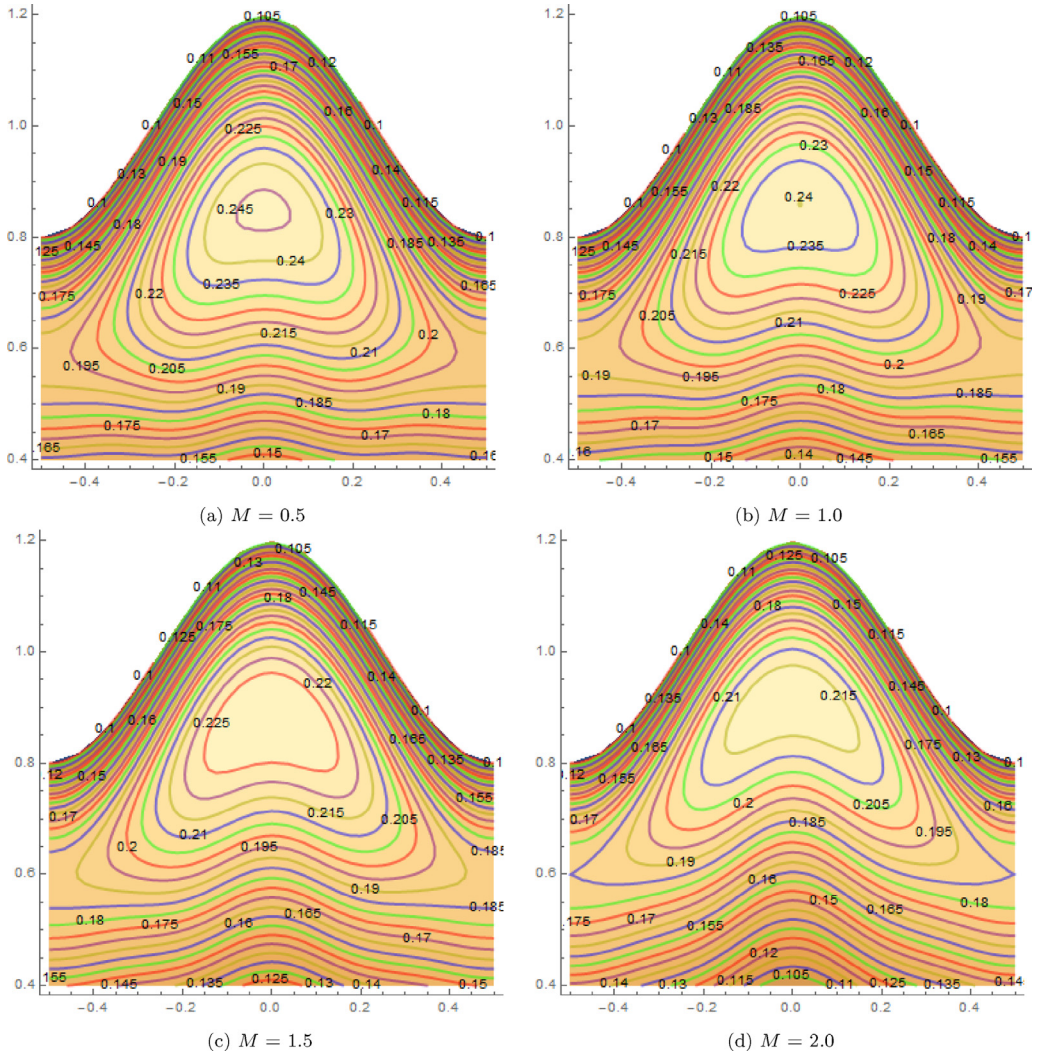

(a) $M = 0.5$ (b) $M = 1.0$ (c) $M = 1.5$ (d) $M = 2.0$

Fig. 9. Streamlines for different values of M and other parameters are ($\alpha = 0.4$, $\phi = 0.2$, $R_e = 0.1$, $\sigma = 0.1$, $\beta = 0.1$, $Q = 0.1$).

Since $L_y^{-1}(*) = \underbrace{\int_0^y (*)dy}_{4-times}$.

So, now we can decompose ψ as:

$$\psi = \sum_{n=0}^{\infty} \psi_n. \tag{23}$$

Substituting ψ into Eq. (22), and using the boundary Eqs. (21), we obtain:

$$\psi_0 = y\left(\frac{\eta(x)+3q}{2\eta(x)}\right) - y^3\left(\frac{\eta(x)+q}{2\eta^3(x)}\right),$$

$$\psi_{(n\geq 1)} = \Phi_{y,n} + L_y^{-1}\left(R_e\alpha\left[\left(\frac{\partial\psi_{n-1}}{\partial y}\right)\left(\frac{\partial^3\psi_{n-1}}{\partial x\partial y^2} + \alpha^2\frac{\partial^3\psi_{n-1}}{\partial x^3}\right) - \left(\frac{\partial\psi_{n-1}}{\partial x}\right)\left(\frac{\partial^3\psi_{n-1}}{\partial y^3} + \alpha^2\frac{\partial^3\psi_{n-1}}{\partial x^2\partial y}\right)\right]\right)$$
$$-L_y^{-1}\left(\left[\alpha^4\frac{\partial^4\psi_{n-1}}{\partial x^4} + 2\alpha^2\frac{\partial^4\psi_{n-1}}{\partial x^2\partial y^2}\right] + M^2\frac{\partial^2\psi_{n-1}}{\partial y^2} + \frac{1}{\sigma}\left(\frac{\partial^2\psi_{n-1}}{\partial y^2} + \alpha^2\frac{\partial^2\psi_{n-1}}{\partial x^2}\right)\right),$$

since $\Phi_{y,n} = c_{0,n}(x) + yc_{1,n}(x) + y^2c_{2,n}(x) + y^3c_{3,n}(x)$, (24)

where $c_{0,n}, c_{1,n}, c_{2,n}, c_{3,n}$ are the integration constants which are evaluated from the given conditions.

Then the solution of the stream function written as:

$$\psi = \sum_{n=0}^{\infty}\psi_n = \psi_0 + \psi_1 + \cdots = A_1(x)y + A_2(x)y^3 + A_3(x)y^5 + A_4(x)y^7 + A_5(x)y^9 + \cdots, \tag{25}$$

where $A_1(x)$, $A_2(x)$, $A_3(x)$, $A_4(x)$ and $A_5(x)$ are written in detail in appendix. From Eqs. (19) and (25) we get the approximate form for the velocity.

By Substituting from Eq. (19) in Eqs. (15), (16) we get the pressure gradient terms in dimensionless form as.

$$\frac{\partial p}{\partial x} = R_e\alpha\left[\left(\frac{\partial\psi}{\partial x}\frac{\partial^2\psi}{\partial y^2}\right) - \left(\frac{\partial\psi}{\partial y}\frac{\partial^2\psi}{\partial x\partial y}\right)\right] - \frac{\partial\omega}{\partial y} - \left(M^2 + \frac{1}{\sigma}\right)\left(\frac{\partial\psi}{\partial y} + 1\right),$$

$$\frac{\partial p}{\partial y} = R_e\alpha^3\left[\left(\frac{\partial\psi}{\partial y}\frac{\partial^2\psi}{\partial x^2}\right) - \left(\frac{\partial\psi}{\partial x}\frac{\partial^2\psi}{\partial x\partial y}\right)\right] + \alpha^2\frac{\partial\omega}{\partial x} + \frac{\alpha^2}{\sigma}\frac{\partial\psi}{\partial x}. \tag{26}$$

From these equation and by substituting of ψ and ω we can get the value of the pressure gradients.

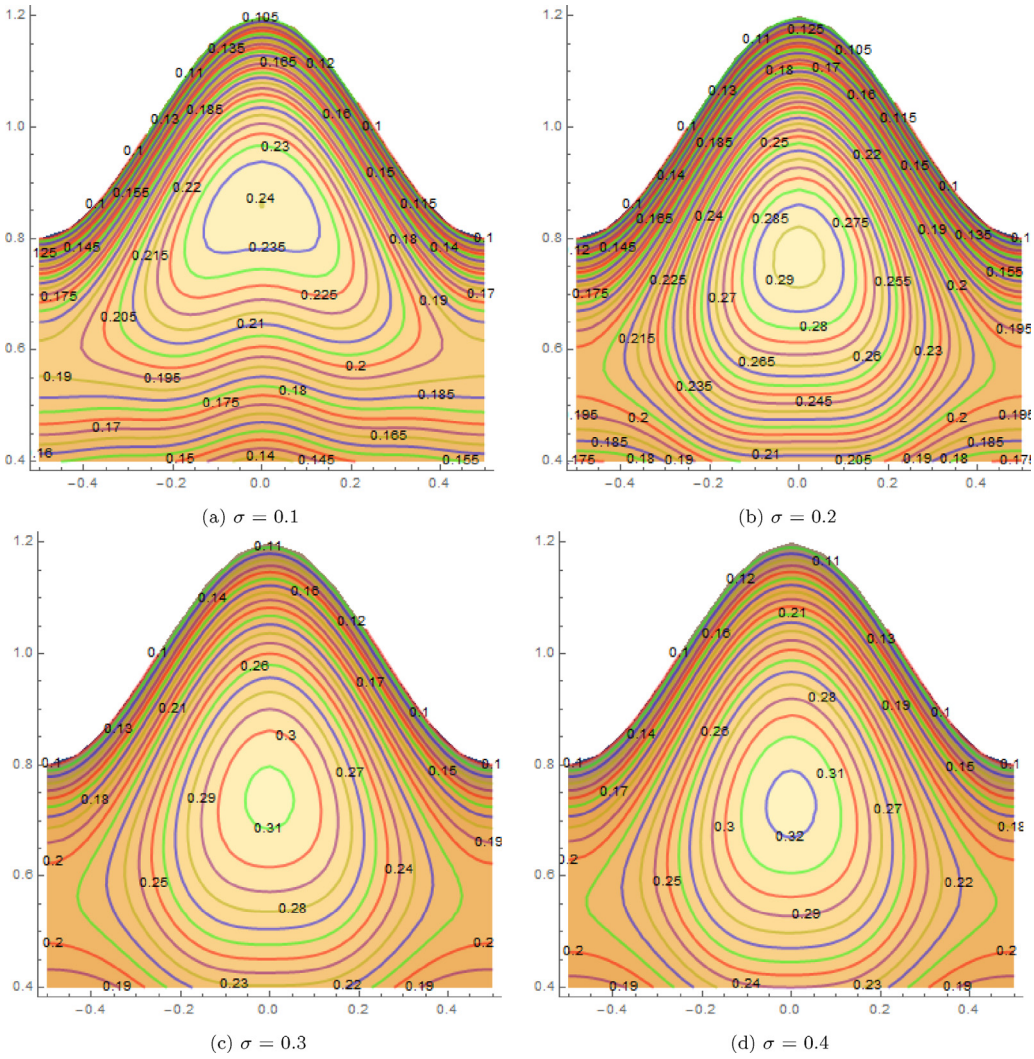

(a) $\sigma = 0.1$ (b) $\sigma = 0.2$ (c) $\sigma = 0.3$ (d) $\sigma = 0.4$

Fig. 10. Streamlines for different values of σ and other parameters are ($\alpha = 0.4$, $\phi = 0.2$, $R_e = 0.1$, $M = 1$, $\beta = 0.01$, $Q = 0.1$).

5. Numerical results and discussion

We divide this section into three subsections. In the first subsection, the effects of various parameters on the velocity characteristics are investigated. Pressure gradient characteristics are discussed in the second subsection. Finally the trapping phenomenon is illustrated in the last subsection.

5.1. Velocity characteristics

This subsection describes the influences of various emerging parameters of our analysis on the fluid velocity components u and v. The behavior of the longitude velocity (u) for values of α, β, M, σ, ϕ, R_e and Q is illustrated in Fig. 3, which shows that the behavior of longitude velocity near the wavy walls and at the center is not similar in view of all parameters. The longitude velocity field increases due to the increase in M, β near the channel walls while it decreases at the center of the channel. However, a reversed trend appears for the effect of the others parameters α, σ, ϕ, R_e and Q. So, the axial velocity is smaller for a magneto-fluid and cilia walls, while it is higher for a porous medium. Also, as expected u is an increasing function with α, ϕ, R_e and Q

As a special case, we compare our results(in the absence of magnetic field, permeability and $\beta = 0$)with ADM method with those obtained by Mekheimer [10] in the case of no magnetic field and couple stresses. Such a comparison is illustrated in Table 1 and Fig. 2, where we notice that the two solutions are coincide across the channel region.

The behavior of the vertical velocity v for several values of α, β, M, σ, ϕ, R_e and Q is elucidates in Fig. 4, and as expected the vertical velocity vanishes at the channel center and behaves as a sinusoidal wave across the channel region. Also, we observe from this Figure that The vertical velocity value decreases with the porosity parameter σ. However, this value increases with the increase of ϕ, R_e, M, β and Q.

5.2. Pumping characteristics

Fig. 5a illustrate that the axial pressure gradient $\frac{\partial p}{\partial x}$ has a periodic nature and it has a decreasing effect on the wider region of the channel where, it over the ranges of $-0.5 \leq x \leq -0.2$, $0.2 \leq$

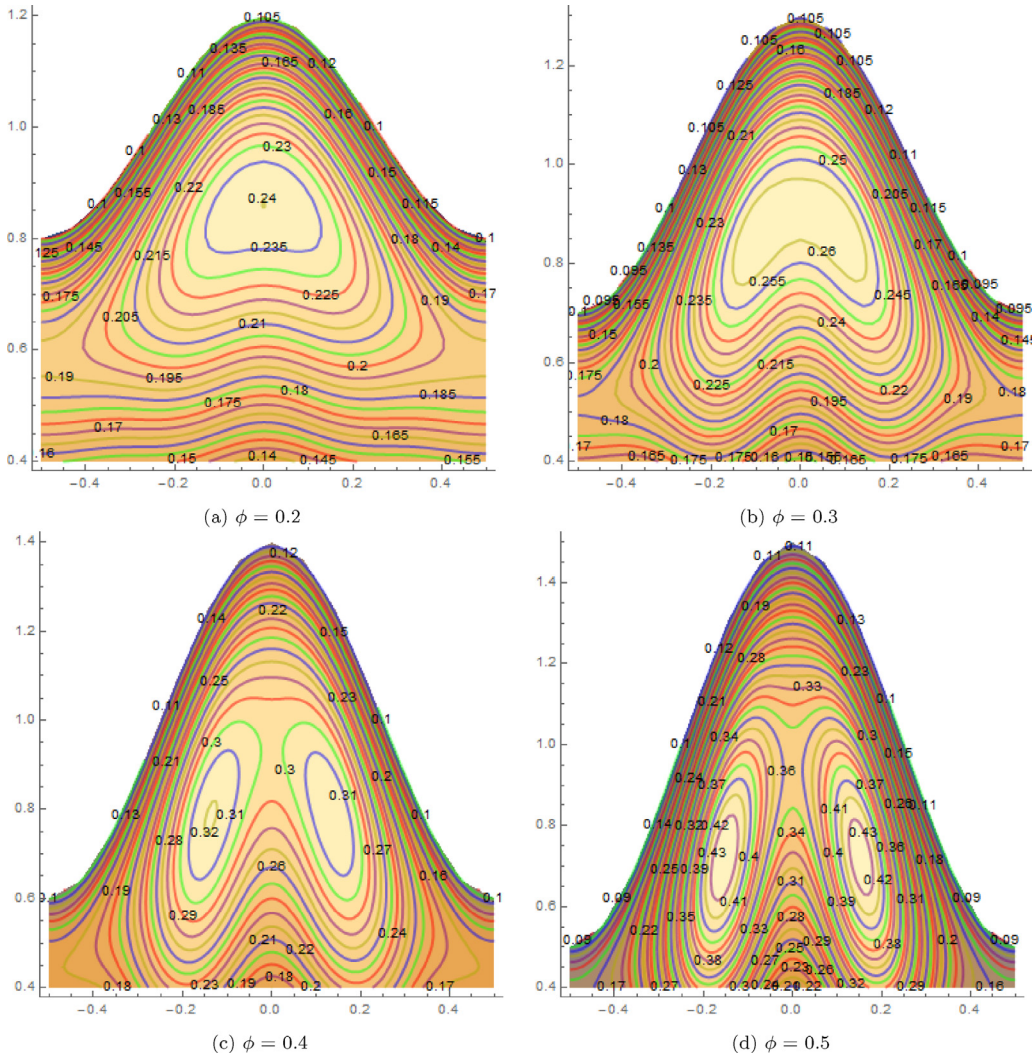

(a) $\phi = 0.2$ (b) $\phi = 0.3$ (c) $\phi = 0.4$ (d) $\phi = 0.5$

Fig. 11. Streamlines for different values of ϕ and other parameters are ($\alpha = 0.4$, $\sigma = 0.1$, $R_e = 0.1$, $M = 1$, $\beta = 0.01$, $Q = 0.1$).

$x \leq 0.5$ approximately. Generally, the pressure gradient attains its maximum value at the narrow region of the channel from where it decreases rapidly as we go to the wider parts. Also, Fig. 5a elucidates that $\frac{\partial p}{\partial x}$ is strongly effected by the cilia walls which has an increasing effect on it. On the other hand, $\frac{\partial p}{\partial x}$ has an increasing effect with σ, ϕ and a decreasing effect with α, M, R_e and Q.

In Fig. 6 the distribution of the vertical pressure gradient $\frac{\partial p}{\partial y}$ is slightly antisymmetric about the midsection and vanishes at the center line $y = 0$. in all figures. Also, $\frac{\partial p}{\partial y}$ takes negative and positive values in both regions of the half channel and behaves as a sinusoidal wave across the channel with large values of the Reynolds number Re and wave number α . Finally the effect of the problem parameter are illustrated in these figures, where the $\frac{\partial p}{\partial y}$ amplitude increases as α, β, R_e, M, Q, ϕ increases, and decreases as the porosity parameter σ increases.

5.3. Streamlines and fluid trapping

The formation of an internally circulating bolus of the fluid by closed streamline is called trapping and this trapped bolus pulled ahead along with the peristaltic wave. Figs. 7 and 10 illustrate the streamline graphs for different values of the wave number α and σ respectively. It is observed that the size and number of trapped bolus increases by increasing α and σ. Figs. 8 and 9 show the effects of the Hartmann number β and M on the stream function, it is clear that the size and number of trapped bolus decreases by increasing the eccentricity of the cilia β and M. Fig. 11 illustrates the effects of ϕ with a given fixed set of the other parameters. By increasing the amplitude ratio ϕ the bolus size increases and more bolus are created. To see the effects of Reynolds number R_e, Fig. 12 is plotted. It is observed that for small values of R_e the bolus appears in the center region and moves towards left and increases in it's size and number as the Reynolds number R_e increases.

6. Concluding remarks

This section is concerned with the major findings from the discussion of the influence of a magneto-fluid through a Darcy flow model with oscillatory wavy walled whose inner surface is ciliated. The problem solution is based on the Adomian Decomposition Method without any used approximations. The main points of the performed analysis are summarized as follows:

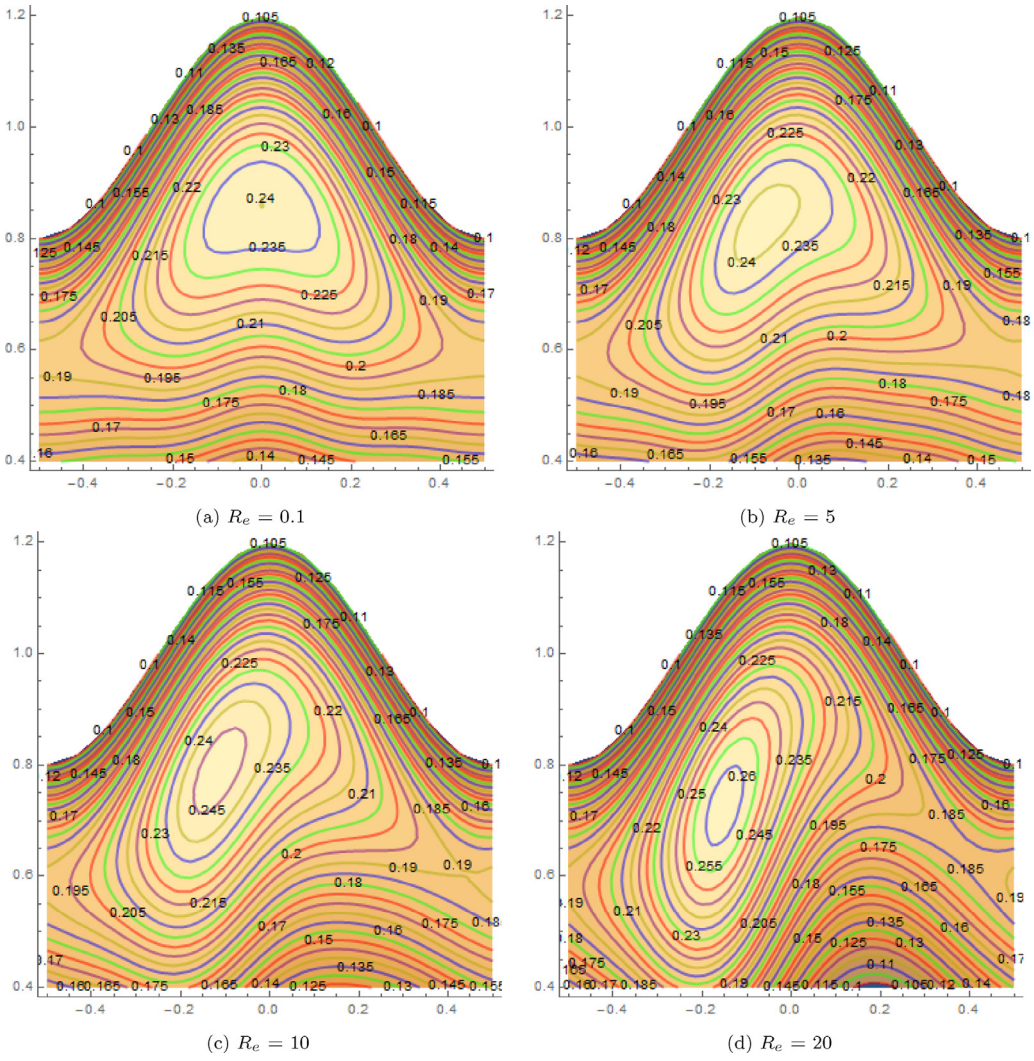

(a) $R_e = 0.1$ (b) $R_e = 5$

(c) $R_e = 10$ (d) $R_e = 20$

Fig. 12. Streamlines for different values of R_e and other parameters are ($\alpha = 0.4$, $\phi = 0.2$, $\sigma = 0.1$, $M = 1$, $\beta = 0.01$, $Q = 0.1$).

1. The Adomian Decomposition Method is able to solve the problems of peristaltic transport without any approximation on the magnitudes of the wave number α, amplitude ratio ϕ and Reynolds number R_e.
2. The longitude velocity field is higher in the absent of the eccentricity of the cilia elliptic path β at the center of the channel while opposite behaviour is shown near the ciliated channel walls.
3. The velocity field increases due to the increase in M near the ciliated channel walls while it decreases at the center of the channel.
4. The magnitude of the pressure gradient in both directions $\frac{\partial p}{\partial x}$, $\frac{\partial p}{\partial y}$ are higher for a ciliated walls than that without a ciliated channel walls .
5. More of trapped bolus numbers in the absent of the eccentricity of the cilia elliptic path β.

Acknowledgement

Authors are very grateful to the anonymous referees for valuable remarks and comments which significantly contributed to the quality of the paper.

Appendix

$$A_1(x) = \left[\frac{1}{6720\sigma\eta(x)}\right][-3\eta(x)^2(\alpha(-2\sigma G'(x)(\alpha\eta'(x)(\alpha\eta'(x)(3QR_e+128\alpha\eta'(x))+224)+20QR_e)+12\eta'(x)(\alpha^2(-R_e)$$
$$\times\sigma(G(x)-1)^2\eta'(x)^2-2R_e\sigma(G(x)-1)^2-2\alpha Q\eta'(x))-2\alpha\sigma(G(x)-1)\eta'(x)(3\alpha\eta'(x)(QR_e+64\alpha\eta'(x))+112)$$
$$+\alpha^2Q\sigma\eta^{(3)}(x)(23QR_e+96\alpha\eta'(x))+72\alpha^3Q\sigma\eta'(x)^2)+56(M^2Q\sigma+Q))+\eta(x)^3(G(x)(\alpha(4R_e\sigma G'(x)(5\alpha^2\eta'(x)^2$$
$$+12)+\alpha^2(-\sigma)(5QR_e\eta^{(3)}(x)-4\eta'(x)(R_e\eta''(x)-48\alpha\eta^{(3)}(x))+144\alpha\eta''(x)^2)+48\alpha\eta'(x)^2)+168(M^2\sigma+1))$$
$$-\alpha(\alpha(\sigma(336G''(x)-\alpha(5QR_e\eta^{(3)}(x)+60\alpha Q\eta^{(4)}(x)+144\alpha\eta''(x)^2))+\alpha\sigma\eta'(x)(51QR_eG''(x)+2R_e\eta''(x)-192$$
$$\times\alpha\eta^{(3)}(x))+48\eta'(x)^2(6\alpha^2\sigma G''(x)+1)+60Q\eta''(x))+\sigma G'(x)(\alpha^2(3\eta''(x)(17QR_e+192\alpha\eta'(x))+20R_e\eta'(x)^2)$$
$$+48R_e))-2\alpha^3R_e\sigma G(x)^2\eta'(x)\eta''(x)-168(M^2\sigma+1))+\alpha^2\eta(x)^4(-23\alpha QR_e\sigma G^{(3)}(x)+96\alpha^2\sigma G''(x)\eta''(x)-28$$
$$\times\alpha R_e\sigma G'(x)^2\eta'(x)+4G'(x)(\alpha\sigma(16\alpha\eta^{(3)}(x)-5R_E(G(x)-1)\eta''(x))-8\eta'(x))+4\alpha\sigma\eta'(x)(16\alpha G^{(3)}(x)-R_e$$
$$\times(G(x)-1)G''(x))-2\alpha R_e\sigma G(x)^2\eta^{(3)}(x)+4\alpha R_e\sigma G(x)\eta^{(3)}(x)+16\alpha^2\sigma(G(x)-1)\eta^{(4)}(x)-16G(x)\eta''(x)-2\alpha$$
$$\times R_e\sigma\eta^{(3)}(x)+16\eta''(x))+\alpha^2\eta(x)^5(\alpha\sigma(20\alpha G^{(4)}(x)+3R_e(G(x)-1)G^{(3)}(x))+G''(x)(-3\alpha R_e\sigma G'(x)-20))$$
$$+3\sigma\eta(x)(3\alpha^2Q\eta''(x)(\alpha\eta'(x)(29QR_e+16\alpha\eta'(x))-112)-2(G(x)-1)(\alpha\eta'(x)(\alpha\eta'(x)(\alpha\eta'(x)(3QR_e+160\alpha\eta'(x))$$
$$+336)+44QR_e)+560))+24Q\sigma(\alpha\eta'(x)(4\alpha\eta'(x)(\alpha\eta'(x)(9\alpha\eta'(x)-2QR_e)+42)+15QR_e)+420)]$$

$$A_2(x) = \left[\frac{1}{5040\sigma\eta(x)^3}\right][3\eta(x)^2(-2\alpha\sigma G'(x)(8\alpha\eta'(x)(\alpha\eta'(x)(QR_e+18\alpha\eta'(x))+42)+33QR_e)+16\alpha(\eta'(x)(\alpha^2(-R_r)\sigma$$
$$\times(G(x)-1)^2\eta'(x)^2-3R_e\sigma(G(x)-1)^2-3\alpha Q\eta'(x))+\alpha\sigma(G(x)-1)\eta''(x)(\alpha\eta'(x)(QR_e-27\alpha\eta'(x))-21)+9\alpha^3$$
$$\times Q\sigma\eta''(x)^2)+84(M^2Q\sigma+Q)+\alpha^3Q\sigma\eta^{(3)}(x)(41QR_e+192\alpha\eta'(x)))+\eta(x)^3(\alpha^2(\sigma(504G''(x)+\alpha(7QR_e\eta^{(3)}(x)$$
$$-99\alpha Q\eta^{(4)}(x)-162\alpha\eta''(x)^2))+\alpha\sigma\eta'(x)(75QR_eG''(x)+11R_e\eta''(x)-216\alpha\eta^{(3)}(x))+54\eta'(x)^2(6\alpha^2\sigma G''(x)+1)$$
$$+99Q\eta''(x))+G(x)(-2\alpha(\sigma(R_eG'(x)(10\alpha^2\eta'(x)^2+27)+\alpha^2\eta''(x)(11R_e\eta'(x)-81\alpha\eta''(x)))+27\alpha\eta'(x)^2)-252(M^2$$
$$\times\sigma+1)+\alpha^3\sigma\eta^{(3)}(x)(216\alpha\eta'(x)-7QR_e))+\alpha\sigma G'(x)(\alpha^2(3\eta''(x)(25QR_e+216\alpha\eta'(x))+20R_e\eta'(x)^2)+54R_e)$$
$$+11\alpha^3R_e\sigma G(x)^2\eta'(x)\eta''(x)+252(M^2\sigma+1))+\alpha^2\eta(x)^4(41\alpha QR_e\sigma G^{(3)}(x)-108\alpha^2\sigma G''(x)\eta''(x)+34\alpha R_e\sigma G'(x)^2$$
$$\times\eta'(x)+4G'(x)(\alpha\sigma(5R_e(G(x)-1)\eta''(x)-18\alpha\eta^{(3)}(x))+9\eta'(x))-2\alpha\sigma\eta'(x)(36\alpha G^{(3)}(x)-R_e(G(x)-1)G''(x))$$
$$+\alpha R_e\sigma G(x)^2\eta^{(3)}(x)-2\alpha R_e\sigma G(x)\eta^{(3)}(x)-18\alpha^2\sigma(G(x)-1)\eta^{(4)}(x)+18G(x)\eta''(x)+\alpha R_e\sigma\eta^{(3)}(x)-18\eta''(x))$$
$$+\alpha^2\eta(x)^5(\alpha\sigma(-33\alpha G^{(4)}(x)-8R_e(G(x)-1)G^{(3)}(x))+G''(x)(8\alpha R_e\sigma G'(x)+33))+3\sigma\eta(x)(-2(G(x)-1)(-\alpha$$
$$\times\eta'(x)(4\alpha\eta'(x)(\alpha\eta'(x)(45\alpha\eta'(x)-2QR_e)+126)+81QR_e)-420)-9\alpha^2Q\eta''(x)(\alpha\eta'(x)(19QR_e+48\alpha\eta'(x))$$
$$-56))+6Q\sigma(-\alpha\eta'(x)(\alpha\eta'(x)(\alpha\eta'(x)(36\alpha\eta'(x)-65QR_e)+1008)+99QR_e)-420)]$$

$$A_3(x) = \left[\frac{1}{480\sigma\eta(x)^5}\right][-3\alpha^3QR_e\sigma G^{(3)}(x)\eta(x)^4-3\eta(x)^2(2\alpha(-\alpha Q\eta'(x)^2(\alpha R_e\sigma G'(x)+2)-2QR_e\sigma G'(x)-2\sigma\eta'(x)(8\alpha$$
$$\times G'(x)+R_e(G(x)-1)^2)+\alpha\sigma(G(x)-1)\eta''(x)(3\alpha QR_e\eta'(x)-8)+6\alpha^3Q\sigma\eta''(x)^2)+4(M^2Q\sigma+Q)+\alpha^3Q\sigma\eta^{(3)}(x)$$
$$\times(3QR_e+16\alpha\eta'(x)))+3\eta(x)^3(-\alpha^2(\sigma G''(x)(\alpha QR_e\eta'(x)+8)+Q\eta''(x)(\alpha R_e\sigma G'(x)+2)+\alpha QR_e\sigma\eta^{(3)}(x))+G(x)$$
$$\times(4M^2\sigma+\alpha^3QR_e\sigma\eta^{(3)}(x)+4)-4(M^2\sigma+1)+2\alpha^4Q\sigma\eta^{(4)}(x))+\alpha^2\eta(x)^5(\alpha\sigma(2\alpha G^{(4)}(x)+R_e(G(x)-1)G^{(3)}(x))$$
$$+G''(x)(\alpha(-R_e)\sigma G'(x)-2))+9\alpha\sigma\eta(x)(2(G(x)-1)\eta'(x)(\alpha\eta'(x)(\alpha QR_e\eta'(x)-8)-2QR_e)+\alpha Q\eta''(x)(\alpha\eta'(x)$$
$$\times(5QR_e+24\alpha\eta'(x))-8))-36\alpha Q\sigma\eta'(x)(\alpha\eta'(x)(\alpha\eta'(x)(QR_e+4\alpha\eta'(x))-8)-QR_e)]$$

$$A_4(x) = \left[\frac{1}{1680\sigma\eta(x)^7}\right][\alpha(3\eta(x)^2(-4\alpha Q\eta'(x)^2(\alpha R_e\sigma G'(x)+1)-2QR_e\sigma G'(x)+4\alpha^2\sigma\eta'(x)^3(8\alpha G'(x)+R_e(G(x)-1)^2)$$
$$+4\alpha^2\sigma(G(x)-1)\eta'(x)\eta''(x)(5QR_e+12\alpha\eta'(x))-4R_e\sigma(G(x)-1)^2\eta'(x)+\alpha^2Q\sigma\eta^{(3)}(x)(3QR_e+16\alpha\eta'(x))+12\alpha^3$$
$$\times Q\sigma\eta''(x)^2)-3\eta(x)^3(\alpha(\alpha\sigma\eta'(x)(QR_eG''(x)+(G(x)-1)(3R_e(G(x)-1)\eta''(x)+8\alpha\eta^{(3)}(x)))-2\eta'(x)^2(-6\alpha^2\sigma$$
$$\times G''(x)+G(x)-1)+\alpha Q\sigma(3R_e(G(x)-1)\eta^{(3)}(x)+\alpha\eta^{(4)}(x))+6\alpha^2\sigma(G(x)-1)\eta''(x)^2-Q\eta''(x))+\sigma G'(x)(-2R_e$$
$$\times G(x)+\alpha^2\eta''(x)(QR_e+24\alpha\eta'(x))+2R_e))+\alpha\eta(x)^4(3\alpha QR_e\sigma G^{(3)}(x)+12\alpha^2\sigma G''(x)\eta''(x)-6\alpha R_e\sigma G'(x)^2\eta'(x)$$
$$-4G'(x)(\eta'(x)-2\alpha^2\sigma\eta^{(3)}(x))+2\alpha\sigma\eta'(x)(4\alpha G^{(3)}(x)+R_e(G(x)-1)G''(x))+\alpha R_e\sigma G(x)^2\eta^{(3)}(x)-2\alpha R_e\sigma G(x)$$
$$\times\eta^{(3)}(x)+2\alpha^2\sigma(G(x)-1)\eta^{(4)}(x)-2G(x)\eta''(x)+\alpha R_e\sigma\eta^{(3)}(x)+2\eta''(x))+\alpha\eta(x)^5(\alpha\sigma(-\alpha G^{(4)}(x)-2R_e(G(x)$$
$$-1)G^{(3)}(x))+G''(x)(2\alpha R_e\sigma G'(x)+1))+3\sigma\eta(x)\eta'(x)(-10(G(x)-1)(2\alpha^2\eta'(x)^2(QR_e+2\alpha\eta'(x))-QR_e)-3\alpha^2$$
$$\times Q\eta''(x)(7QR_e+40\alpha\eta'(x)))+18Q\sigma\eta'(x)(\alpha^2\eta'(x)^2(3QR_e+20\alpha\eta'(x))-QR_e))]$$

$$A_5(x) = \left[-\frac{R_e}{4032\eta(x)^9}\right][\alpha^3(3\eta(x)^2(-2QG'(x)\eta'(x)^2 + 14Q(G(x)-1)\eta'(x)\eta''(x) + 4(G(x)-1)^2\eta'(x)^3 + Q^2\eta^{(3)}(x))$$
$$-\eta(x)^3(\eta'(x)(3QG''(x) + 14(G(x)-1)^2\eta''(x)) + G'(x)(4(G(x)-1)\eta'(x)^2 + 3Q\eta''(x)) + 5Q(G(x)-1)\eta^{(3)}(x))$$
$$+\eta(x)^4(QG^{(3)}(x) + 4(G(x)-1)G''(x)\eta'(x) + 4(G(x)-1)G'(x)\eta''(x) - 4G'(x)^2\eta'(x) + 2(G(x)-1)^2\eta^{(3)}(x))$$
$$+\eta(x)^5(G'(x)G''(x) - (G(x)-1)G^{(3)}(x)) + 3Q\eta(x)\eta'(x)(-14(G(x)-1)\eta'(x)^2 - 9Q\eta''(x)) + 24Q^2\eta'(x)^3)]$$

References

[1] A.H. Shapiro, M.Y. Jaffrin, S.L. Weinberg, Peristaltic pumpuing with long wave lengths at low Reynolds number, J. Fluid Mech. 37 (1969) 799–825.
[2] R. Ellahi, M.M. Bhatti, I. Pop, Effects of hall and ion slip on MHD peristaltic flow of jeffrey fluid in a non-uniform rectangular duct, Int. J. Numer. Methods Heat Fluid Flow 26 (6) (2016a) 1802–1820.
[3] R. Ellahi, M.M. Bhatti, C. Fetecau, K. Vafai, Peristaltic flow of couple stress fluid in a non-uniform rectangular duct having compliant walls, Commun. Theor. Phys. 65 (2016b) 66–72.
[4] N.S. Akbar, M. Raza, R. Ellahi, Peristaltic flow with thermal conductivity of H_2O + CU nanofluid and entropy generation, Res. Phys. 5 (2015) 115–124.
[5] E.F. Elshehawey, K.S. Mekheimer, Couple-stresses in peristaltic transport of fluids, J. Phys. D 27 (1994) 1163–1170.
[6] S.N. Elsoud, S.F. Kaldas, K.S. Mekheimer, Interaction of peristaltic flow with pulsatile couple-stress fluid, J. Biomath. 13 (1998) 417–425.
[7] K.S. Mekheimer, E.F.E. Shehawey, A.M. Elaw, Peristaltic motion a of particle fluid suspension in a planar channel, Int. J. Theor. Phys. 37 (1998) 2895–2920.
[8] S. Rashidi, A. Nouri-Borujerdi, M.S. Valipour, R. Ellahi, I. Pop, Stress jump and continuity interface conditions for a cylinder embedded in a porous medium, Transp. Porous Media 107 (1) (2015) 171–186.
[9] K.S. Mekheimer, Y.A. Elmaboud, The influence of heat transfer and magnetic field on peristaltic transport of a newtonian fluid in a vertical annulus, Phys. Lett. A 372 (2008) 1657–1665.
[10] K.S. Mekheimer, Peristaltic flow of blood under effect of a magnetic field in a non uniform channels, Appl. Math. Comput. 153 (2004) 763–777.
[11] K.S. Mekheimer, Effect of the induced magnetic field on peristaltic flow of a couple stress fluid, Phys. Lett. A 372 (2008) 4271–4278.
[12] Y.A. elmaboud, K.S. Mekheimer, A. Abdellatif, Thermal properties of ocouple-stress fluid in an asymmetric channel with peristalsis, J. Heat Transfer 135 (4) (2013) 044502.
[13] R. Ellahi, E. Shivanian, S. Abbasbandy, T. Hayat, Analysis of some magnetohydrodynamic flows of third order fluid saturating porous space, J. Porous Media 18 (2) (2015) 89–98.
[14] N.S. Akbar, M. Raza, R. Ellahi, Influence of induced magnetic field and heat flux with the suspension of carbon nanotubes for the peristaltic flow in a permeable channel, Magn. Magn. Mate. 381 (2015) 405–415.
[15] N.S. Akbar, M. Raza, R. Ellahi, Copper oxide nanoparticles analysis with water as base fluid for peristaltic flow in permeable tube with heat transfer, Comput. Methods Programs Biomed. 130 (2016) 22–30.
[16] S. Takabatake, K. Ayukawa, Numerical study of two dimensional peristaltic flows, J. Fluid Mech. 122 (1982) 439–465.
[17] K.S. Mekheimer, K.A. Hemada, K.R. Raslan, R.E. Abo-Elkhair, A.M.A. Moawad, Numerical study of a non-linear peristaltic transport: application of Adomian decomposition method(ADM), Gen. Math. Notes 20 (2014) 22–49.
[18] K.S. Mekheimer, Non linear peristaltic transport of magneto-hydrodynamic flow in an inclined planner channels, Arab. J. Sci. Eng. 28 (2003) 183.
[19] T. Hayat, A. Ambreen, M. Khan, S. Asghar, Peristaltic transport of a third order fluid under the effect of a magnetic field, Appl. Math. Comput. 53 (2007) 1074.
[20] T. Hayat, N. Ali, Peristaltically induced motion of MHD third grade fluid in a deformable tube, Phys. A. 370 (2006) 225.
[21] T. Hayat, F.M. Mahomed, S. Asghar, Peristaltic flow of a magnetohydrodynamic Johnson–Segalman fluid, Nonlinear Dyn. 40 (2005) 375.
[22] A.E. Scheidegger, The Physics of Flow through Porous Media, third ed., University of Toronto Press, Toronto, Canada, 1974.
[23] C.L. Varshney, The fluctuating flow of a viscous fluid through a porous medium bounded by a porous and a horizontal surface, Indian J. Pure Appl. Math. 10 (1979) 1558.
[24] A. Rapits, C. Perdikis, Flow of a viscous fluid through a porous medium bounded by a vertical surface, Int. J. Eng. Sci. 27 (1983) 1327–1330.
[25] N.T. El-Dabe, S.M. El-Mohendis, Magnetohydrodynamic flow of a second order fluid through a porous medium on an inclined porous plate, Arabian J. Sci. Eng. 20 (1995) 571.
[26] M.A. Sleigh, The Biology of Cilia and Flagella, MacMillian, New York, 1962.
[27] S. Gullapalli, M. Wong, Nanotechnology: a guide to nano-objects, Chem. Eng. Prag. 107 (5) (2011) 28–32.
[28] Q. Xue, Model for thermal conductivity of carbon nanotube-based composites, Mod. Phys. Lett. B 368 (2005) 302–307.
[29] N.S. Akbar, A.W. Butt, CNT suspended nanofluid analysis in a flexible tube with ciliated walls, Eur. Phys. J. Plus 129 (2014) 174.
[30] N.S. Akbar, Z.H. Khan, S. Nadeem, Metachronal beating of cilia under influence of hartmann layer and heat transfer, Eur. Phys. J. Plus 129 (2014) 176.
[31] N.S. Akbar, S. Nadeem, Exact solution of peristaltic flow of biviscosity fluid in an annulus: a note, Alex. Eng. J. 53 (2014a) 449–454.
[32] N.S. Akbar, S. Nadeem, Simulation of second grade fluid model and heating scheme on the blood flow through a tapered artery with mass transfer, Heat Transfer Res. 45 (2014b) 391–408.
[33] S. Nadeem, E.N. Maraj, N.S. Akbar, Theoretical analysis for peristaltic flow of carreau nano fluid in a cmved channel with compliant walls, J. Comput. Theor. Nanosci. 11 (2014) 1443–1452.
[34] N.S. Akbar, S. Nadeem, Simulation of peristaltic flow of chyme in small intestine for couple stress fluid, Meccanica 49 (2014) 325–334.
[35] H.L. Agrawal, Anawaruddin, Cilia transport of bio-fluid wih variable viscosity, Indian J. Pure Appl. Math. 15 (10) (1984) 1128–1139.
[36] N.S. Akbar, Z.H. Khan, Metachronal beating of cilia under the influence of casson fluid and magnetic field, Appl. Math. Comput. 378 (2015) 320–326.
[37] G. Adomian, Solving Froniter Problems of Physics: The Decomposition Method, Kluwer Academic Publishers, Boston, 1994.
[38] G. Adomian, A review of the decomposition method in applied mathematics, J. Math. Anal. Appl. 135 (1988) 501–544.
[39] A.K. Khalifa, K.R. Raslan, H.M. Alzubaidi, Numerical syudy using ADM for the modified regularized long wave equation, Appl. Math. Model. 32 (2008) 2962–2972.
[40] A.M. Wazwaz, The decompostition method applied to the system of partial differential equations and reaction-diffusion Brusselator model, Appl. Math. Comput. 110 (2000) 251–264.
[41] H.N. Ismail, K. R.Raslan, G.S. Salem, Solitary wave solutions for the general KDV equation by Adomian decomposition method, Appl. Math. Comput. 154 (2004) 17–29.
[42] A.M. Wazwaz, A reliable treatment for mixed Volterra–Fredholm integral equations, Appl. Math. Comput. 127 (2002) 405.
[43] K. Abbaoui, Y. Cherruault, Convergence of Adomian method applied to differential equations, Comput. Math. Appl. 28 (5) (1994) 103–109.
[44] Y. Cheruault, G. Saccomandi, B. Some, New results for convergence of adomain method applied to integral equations, Math. Comput. Model. 16 (2) (1992) 85–93.
[45] K. Abbaoui, Y. Cherruault, New ideas for proving convergence of decomposition methods, Comput. Math. Appl. 29 (7) (1995) 103–108.
[46] T. Hayat, Q. Hussain, N. Ali, Influence of partial slip on the peristaltic flow in a porous medium, Phys. A 387 (2008) 3399–3409.